### Biomedical Physics & Engineering Express



#### **OPEN ACCESS**

#### RECEIVED

10 June 2024

### REVISED

24 July 2024

ACCEPTED FOR PUBLICATION
13 August 2024

#### PUBLISHED

5 September 2024

Original content from this work may be used under the terms of the Creative Commons Attribution 4.0 licence.

Any further distribution of this work must maintain attribution to the author(s) and the title of the work, journal citation and DOI.



### **PAPER**

Characterisation of 3D-printable thermoplastics to be used as tissue-equivalent materials in photon and proton beam radiotherapy end-to-end quality assurance devices

Mariana Bento<sup>1,2,\*</sup>, Hannah Cook<sup>2</sup>, Virginia Marin Anaya<sup>3</sup>, Esther Bär<sup>3</sup>, Andrew Nisbet<sup>1</sup>, Ana Lourenço<sup>1,2</sup>, Mohammad Hussein<sup>1,2</sup>, and Catarina Veiga<sup>1</sup>

- <sup>1</sup> Department of Medical Physics and Biomedical Engineering, University College London, London, United Kingdom
- Radiotherapy and Radiation Dosimetry Group, National Physical Laboratory, Teddington, United Kingdom
- <sup>3</sup> Radiotherapy Physics Services, University College London Hospitals NHS Foundation Trust, London, United Kingdom
- \* Author to whom any correspondence should be addressed.

E-mail: mariana.bento.20@ucl.ac.uk, hannah.cook@npl.co.uk, virginia.marinanaya1@nhs.net, esther.baer@nhs.net, andrew.nisbet@ucl.ac.uk, ana.lourenco@npl.co.uk, mohammad.hussein@npl.co.uk and c.veiga@ucl.ac.uk

Keywords: radiotherapy, proton beam therapy, additive manufacturing, 3D-printing, quality assurance

Supplementary material for this article is available online

### **Abstract**

Objective. To investigate the potential of 3D-printable thermoplastics as tissue-equivalent materials to be used in multimodal radiotherapy end-to-end quality assurance (QA) devices. Approach. Six thermoplastics were investigated: Polylactic Acid (PLA), Acrylonitrile Butadiene Styrene (ABS), Polyethylene Terephthalate Glycol (PETG), Polymethyl Methacrylate (PMMA), High Impact Polystyrene (HIPS) and StoneFil. Measurements of mass density ( $\rho$ ), Relative Electron Density (RED), in a nominal 6 MV photon beam, and Relative Stopping Power (RSP), in a 210 MeV proton pencilbeam, were performed. Average Hounsfield Units (HU) were derived from CTs acquired with two independent scanners. The calibration curves of both scanners were used to predict average  $\rho$ , RED and RSP values and compared against the experimental data. Finally, measured data of  $\rho$ , RED and RSP was compared against theoretical values estimated for the thermoplastic materials and biological tissues. Main results. Overall, good  $\rho$  and RSP CT predictions were made; only PMMA and PETG showed differences >5%. The differences between experimental and CT predicted RED values were also < 5% for PLA, ABS, PETG and PMMA; for HIPS and StoneFil higher differences were found (6.94% and 9.42/15.34%, respectively). Small HU variations were obtained in the CTs for all materials indicating good uniform density distribution in the samples production. ABS, PLA, PETG and PMMA showed potential equivalency for a variety of soft tissues (adipose tissue, skeletal muscle, brain and lung tissues, differences within 0.19%–8.35% for all properties). StoneFil was the closest substitute to bone, but differences were > 10%. Theoretical calculations of all properties agreed with experimental values within 5% difference for most thermoplastics. Significance. Several 3D-printed thermoplastics were promising tissue-equivalent materials to be used in devices for end-to-end multimodal radiotherapy QA and may not require corrections in treatment planning systems' dose calculations. Theoretical calculations showed promise in identifying thermoplastics matching target biological tissues before experiments are performed.

### 1. Introduction

Radiotherapy is one of the most used treatment modalities for cancer, with around 50% of the diagnosed patients being treated with ionising radiation (Baskar *et al* 2012). In the past decades, technological

innovations have allowed for the development of advanced radiotherapy techniques, such as intensity modulated radiation therapy (IMRT) and proton beam therapy (PBT), that deliver highly conformal dose distributions to the tumour volume leading toward improved patient outcomes (Lomax 1999,

Cheung 2006, Palma et al 2008, Stieler et al 2011, Liu and Chang 2011). However, modern radiotherapy techniques require complex treatment plans, associated with additional sources of uncertainties that need to be detected and corrected for (Kutcher et al 1994, Leary et al 2015). Quality assurance (QA) procedures have been implemented in clinical facilities to assess the safety and accuracy of the imaging techniques and planning and delivery of treatments. Within these, endto-end QA evaluates the entire treatment chain, testing the different individual processes and coordination between them along the treatment pathway, by mimicking real clinical scenarios (Schreiner 2019). Comprehensive guidelines for the implementation of QA procedures have been proposed by several national and international bodies including The American Association of Physicists in Medicine (AAPM) task groups (Kutcher et al 1994, Fraass et al 1998, Mutic et al 2003, Arjomandy et al 2019).

Physical phantoms have been widely used for dosimetry verification tests in radiotherapy (McGarry et al 2020). Physical phantoms may consist of simple water tanks, with water being defined as the standard reference material for dosimetry in radiotherapy. Phantoms made of water equivalent materials, i.e., solid water, are a popular alternative since they allow for more time-efficient QA tests (Constantinou et al 1982, Allahverdi et al 1999, Gargett et al 2020). Over time, phantoms have become increasingly complex, with new tissue-equivalent materials, such as resins, gels, thermoplastics and polymers, and anthropomorphic phantoms being developed, accounting for the diversity in tissue types and complex anatomic structures present in the human body (McGarry et al 2020). From the available anthropomorphic phantoms, only a few are suitable to be used for end-to-end QA in photon radiotherapy, without resorting to overrides within the treatment planning system (TPS), as most of the materials used as tissue-equivalent materials are either equivalent for diagnostic or therapeutic beam energies, but not both (McGarry et al 2020). Previous authors have considered a 5% uncertainty limit in the radiological equivalency of a material for it to be adequate for end-to-end QA applications (Grant et al 2014, Lewis et al 2018, Tino et al 2022). At higher energy levels, Compton scattering is the main photon interaction. However, at diagnostic energies, photoelectric effect has a significant contribution to the total photon attenuation. Due to the high dependence of the photoelectric effect cross section on the atomic number (Z), some materials do well at mimicking the attenuation properties of tissues at therapeutic energies but fail under diagnostic energies, when high differences in the elemental compositions are found. Moreover, most tissue-equivalent materials developed were built specifically for dosimetry verification in photon therapy. Therefore, radiological equivalence for end-to-end multimodality radiotherapy (photon and proton therapies) is not guaranteed. Proton

therapy has become an attractive modality of radiation treatment for several cancer types, due to the advantages associated with the steep dose fall-off at the end of these particles' track, described as the Bragg-peak (Paganetti 2012). With proton therapy becoming increasingly available worldwide (Particle Therapy Co-Operative Group (PTCOG) 2024), the development of proton-specific QA procedures is crucial. Most of the available QA tools are photon specific and not suitable for proton range verification (Arjomandy et al 2009, Grant et al 2014, Rana et al 2019, Cook et al 2023). While photon interactions with matter are predicted mostly based on the medium's electron density, for protons the stopping power is the radiological property used for the calculation of dose distributions.

In the past years, efforts have been made in the development of 3D-printed in-house phantoms as an alternative to commercial phantoms (Ehler et al 2014, Yea et al 2017, Kadoya et al 2019, Alexander et al 2022, Cook et al 2022, Tillery et al 2022, Tino et al 2022). The Alderson phantoms (RANDO and ART, Radiology Support Devices Inc., Carson, CA, US), as well as the full-body adult and paediatric ATOM and the E2E SBRT thorax phantoms (Sun Nuclear Inc., Melbourne, FL, US), are examples of very detailed and realistic commercial anthropomorphic models. Even though these phantoms have been shown to perform well as end-to-end QA tools in conventional photon beam therapy, their fabrication processes (e.g., casting and moulding) are associated with high costs of production. Additive manufacturing (AM), or 3D-printing, has become of interest for radiotherapy applications not only in the development of phantoms for a variety of QA protocols (Ehler et al 2014, Ju et al 2014, Burleson et al 2015, Leary et al 2015, Craft and Howell 2017, Oh et al 2017, Tino et al 2019, Rooney et al 2020, Marshall et al 2023, Brunner et al 2024), but also in the manufacturing of bolus, immobilization devices, collimators and compensators. 3D-printing technology offers easy customisation of models, flexibility of design and low costs of production, without compromising on the level of detail and accuracy. Ehler et al (2014) have proposed a 3D-printed head and neck phantom, consisting of a shell made of Acrylonitrile Butadiene Styrene (ABS), filled with a wax material, for patient-specific QA in intensity-modulated radiation therapy (IMRT), with potential applications for an end-to-end QA approach. Van der Walt et al (2019) and Delombaerde et al (2020) found good agreement between measured and CT predicted mass densities for samples printed with Polylactic Acid (PLA), with no overrides required in the TPS during photon dose calculations. Grant et al (2014) found that Polyethylene (PE) and High-Impact Polystyrene (HIPS) were proton-equivalent, with the relative stopping power (RSP) values for these materials being well predicted by HU-RSP calibration curve. Similar results have also been found by Brunner et al (2024) for PLA, ABS and Nylon, with differences between

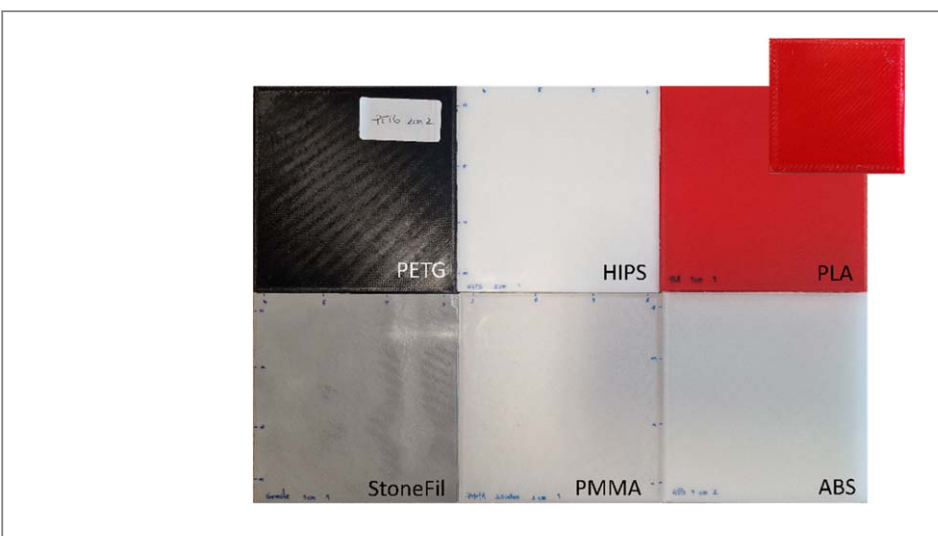


Figure 1. 3D-printed slabs for each thermoplastic. At the top-right corner, a cross-sectional view of the samples core is shown.

measured and CT predicted RSPs within 3%. However, density overrides at the TPS were required in the work conducted by Craft and Howell (2017), on the development of a PLA 3D-printed patient-specific female chest phantom for photon therapy. Burleson et al (2015) have highlighted in their work the impact of the selected printing parameters on the final density of the printed structures. Dancewicz et al (2017) have also reported the existence of air gaps in the prints infill even for the highest infill levels. The presence of air gaps in the prints core will affect the final density of the phantom, as well as its absorption and scattering properties. Zou et al (2015), in their work on the 3Dprinting of an electron bolus made of PLA and using a solid infill, found considerable HU variations measured between samples, and they highlighted the need to understand how inhomogeneities in the 3D-printing process can impact the final properties of the models. These studies suggest that different filament manufacturers and printing conditions (e.g., 3D-printer and printing parameters) can result in models with different densities and radiological properties for the same thermoplastic materials.

Understanding the performance of 3D-printing technology and characterising 3D-printable thermoplastics as tissue-equivalent materials in diagnostic and therapeutic exposures is essential to realise the potential and ensure the safety of this disruptive technology in the clinic. However, the suitability of 3Dprinting materials as tissue-equivalent materials for use in multimodal radiotherapy end-to-end QA devices has yet to be comprehensively explored. In this work, the radiological properties of six commercially available thermoplastic materials were characterised post-printing, both at the diagnostic (CT) and therapeutic (photon and proton) levels. Then, we evaluated the associated CT errors of these materials in the treatment chain and explored their suitability as substitutes for a variety of biological tissues for end-toend multimodal QA devices. We also investigated the

accuracy of theoretical (mathematical) calculations of their radiological properties to guide the selection and development of new tissue-equivalent filaments. This work allowed us to critically evaluate fused deposition modeling (FDM) 3D-printing technology on the development of tissue-equivalent materials for end-to-end QA phantoms, as well as the need for guidance to standardise the use of this manufacturing technique for radiotherapy clinical applications. To the best of our knowledge, this is the first study performing a comprehensive evaluation of a set of commonly used 3D-printable thermoplastics at both diagnostic (CT) and therapeutic (megavoltage photon and proton beams) energies.

### 2. Materials and methods

### 2.1. Sample production

Six thermoplastics were investigated in this study: Polylactic Acid (PLA), Acrylonitrile Butadiene Styrene (ABS), Polyethylene Terephthalate Glycol (PETG), Polymethyl Methacrylate (PMMA), High Impact Polystyrene (HIPS) and StoneFil. For each material, two  $10 \times 10 \times 1 \text{ cm}^3$  and two  $10 \times 10 \times 2 \text{ cm}^3$  slabs were 3D-printed (figure 1).

The 3D-printer Raise3D Pro 2 Plus (Raise 3D Technologies, Inc., CA, USA), together with the Simplify3D (Simplify3D, OH, USA) slicer software (version 4.1.2), were used in the production of the 3D-printed samples. The Raise3D Pro 2 Plus is equipped with two hot-ends for dual extrusion and offers a large building volume of  $305 \times 305 \times 605 \text{ mm}^3$ . To maximise the homogeneity of the samples and minimise the overall volume of air gaps, no infill pattern was selected; instead, each layer consisted of two perimeter shells and the core was filled using the printing feature 'solid layers'. Other printing parameters were empirically fine-tuned to optimise the print quality for every material (table 1). The optimisation was an iterative

**Table 1.** Properties of each thermoplastic material and printing parameters used.

Thermoplastic	PLA	ABS	PETG	PMMA	HIPS	StoneFil
Vendor	Raise 3D technologies	Fillamentum Manufacturing (Czech	Niceshops GmbH	Mitsubishi Chemical	Spectrum Filaments	FormFutura VOF (The
	(CA, USA)	Republic)	(Austria)	(Japan)	(Poland)	Netherlands)
Product name	Premium PLA	ABS Extrafill	3DJAKE PETG	3Diakon <sup>TM</sup> PMMA	HIPS-X	$StoneFil^{TM}$
Filament colour	Red	Transparent	Black	Clear	Gypsum white	Granite
Elemental Composition	$(C_3H_4O_2)$	$(C_{15}H_{17}N)$	$(C_{26}H_{26}O_8)$	$(C_5H_8O_2)$	$(C_{52}H_{62})$	50% PLA 50% stone <sup>b</sup>
Mass density <sup>a</sup> (g cm <sup>-3</sup> )	1.20	1.04	1.27	1.14	1.05	1.70
Extrusion Multiplier	0.90	0.90	0.85	0.95	0.95	1.05
Retraction Distance (mm)	1.5	1.5	3.0	1.5	1.5	2.0
Extruder Temperature (°C)	210	230	235	255	240	230
$Heated\ Bed\ Temperature\ (^{\circ}C)$	60	100	70	107	95	60

<sup>&</sup>lt;sup>a</sup> provided by the vendor.

 $Abbreviations: PLA-Polylactic Acid; ABS-Acrylonitrile \ Butadiene \ Styrene; PETG-Polyethylene \ Terephthalate \ Glycol; PMMA-Polymethyl \ Methacrylate; HIPS-High \ Impact \ Polystyrene.$ 

<sup>&</sup>lt;sup>b</sup> stone: 60% SiO<sub>2</sub>, 13% Al<sub>2</sub>O<sub>3</sub>, 22% Fe<sub>2</sub>O<sub>3</sub>, 5% CaO.

process aimed at finding a set of unique 3D-printing parameters optimal for each material. It consisted of an in-house protocol that used a variety of 3D-printed models designed to evaluate extrusion temperature, first layer quality, oozing and over- and under-extrusion. All prints used a 0.4 mm nozzle, a printing speed of 3600 mm min<sup>-1</sup> and a layer height of 0.2 mm.

The elemental composition considered for each material is an approximation based on a variety of sources (Żenkiewicz *et al* 2009, Mármol *et al* 2010, Salimi *et al* 2017, Chung *et al* 2018, Hassan *et al* 2020, Panneerselvam *et al* 2021, Nakayenga *et al* 2021, Ranakoti *et al* 2022), as vendors often do not provide this information for proprietary reasons.

### 2.2. Experimental measurements

The patient pathway for radiotherapy treatment consists of the acquisition of CT images of the patient, the calculation of the treatment dose distribution using TPS software and the delivery of the plan. The planning CT scan provides a measure of the attenuation coefficients at diagnostic energy levels (Hounsfield Units, HU), which are calibrated to the physical (mass density,  $\rho$ ) and radiological (relative electron density, RED, and relative stopping power, RSP) properties of the imaged tissues. These properties are then used by the TPS during dose calculations to predict photon attenuation and proton range values. Measurements were performed on all 3D-printed samples to evaluate their physical density and radiological properties, under diagnostic (photons) and treatment (photons and protons) energies, described in the following sections.

### 2.2.1. Mass density

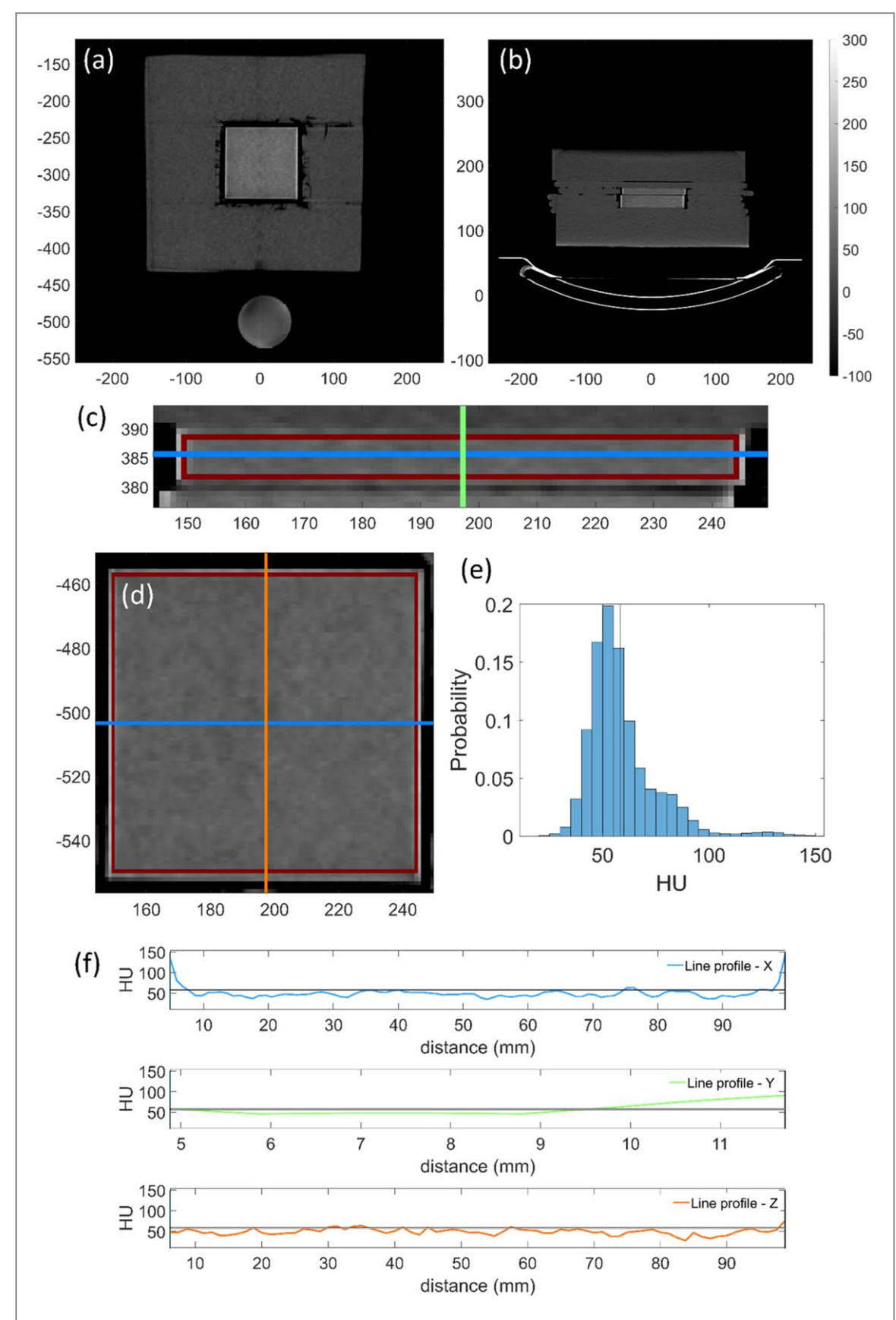
The density of the 3D-printed samples will differ from the density of the filament as provided by the vendor due to the choice of printing parameters (e.g., extrusion multiplier, infill type and percentage), which are typically tuned to achieve the best printing quality. The  $\rho$  of each sample was calculated from volume and mass measurements. The volume was derived from length, width, and height measurements taken for each sample using a digital calliper (Premier Farnell Limited, UK), with resolution 0.01 mm. Mass measurements were performed with a precision balance (model MW723i-M, Bel Engineering Ltd., UK) with resolution 0.001 g.

2.2.2. Radiological properties at diagnostic energy levels The 3D-printed slabs were scanned in two independently commissioned CT systems at two different institutions. The first was the AnyScan TRIO® SPECT/CT (Mediso Medical Imaging Systems, Hungary) installed at the National Physical Laboratory, operating at 300 mAs and 120 kVp; images were reconstructed with the default abdominal settings (convolution kernel F0060N+003BofH) and a slice

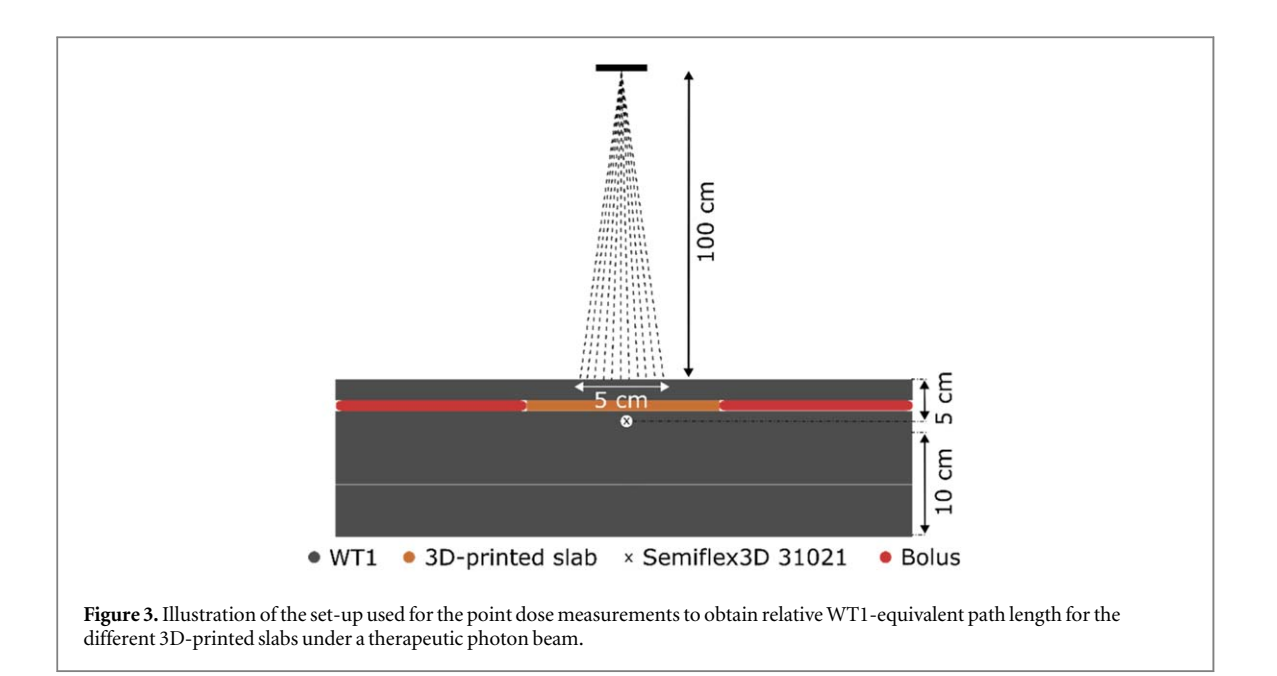
thickness of 1.25 mm. The second was the Philips Spectral CT 7500 (Koninklijke Philips N.V, Netherlands) installed at University College London Hospitals NHS Foundation Trust, operating at 455 mAs and 120 kVp; images were reconstructed with the default abdominal settings (convolution kernel IMR2) and a slice thickness of 2 mm. The slabs were positioned on the treatment couch in groups (1 cm slab with a 2 cm slab of the same material) and surrounded by bolus material and 5 cm of solid water slabs both on top and on the bottom (figure 2). For each material, average HU were extracted from the CT scans using the active contour segmentation mode from ITK-Snap (version 3.6.0, Yushkevich et al 2006). A box-shaped segmentation was performed to define a region of interest (ROI) for analysis. This contained only the core of the slabs and excluded their perimeter layers. Figure 2 shows an example of the CT scan of one of the slabs, ROI and line profiles. The HU inside the ROIs were extracted and averaged across the four samples available for each material.

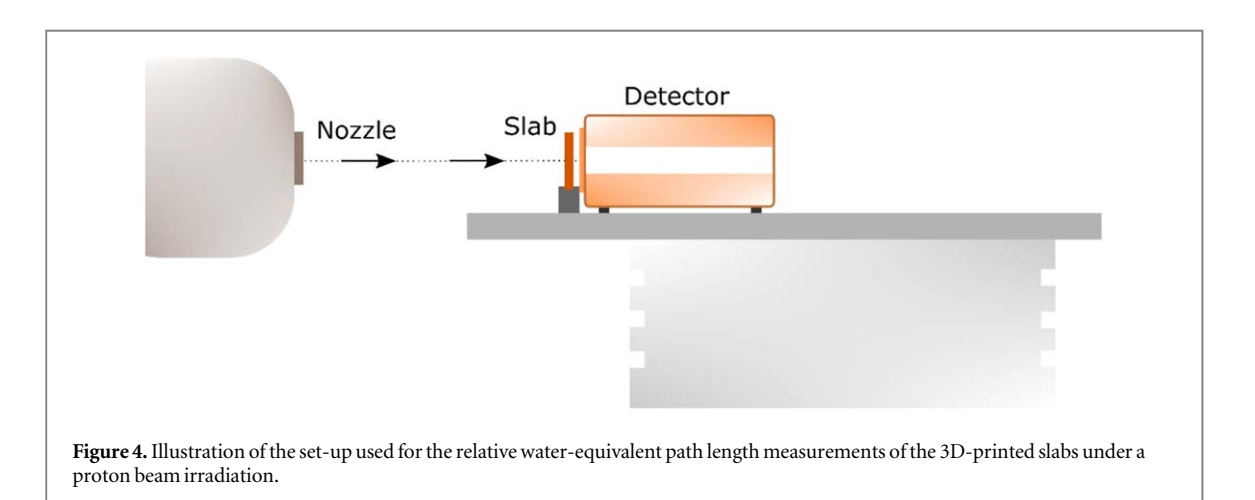
2.2.3. Radiological properties at therapeutic energy levels Water-equivalent path length measurements were performed at therapeutic beam energies to obtain experimental RED and RSP values of each thermoplastic. There is a one-to-one relationship between REDs and RSPs and relative water-equivalent path length since this measure is linearly related with the electron density and stopping power of the medium (Schneider et al 1996, Zhang and Newhauser 2009, Moutrie et al 2015, Dancewicz et al 2017). The 3Dprinted slabs were irradiated with a 6 MV photon beam and a single-spot 210 MeV proton beam. A single energy was considered for both radiation modalities since other studies have reported the waterequivalent path length to be energy independent at megavoltage energies (Lewis et al 2018, Gargett et al 2020).

The MV photon beam irradiations were performed on the Elekta VersaHD LINAC (Elekta, Sweden) installed at the National Physical Laboratory using a PTW Semiflex3D Type 31021 ionisation chamber (PTW Freiburg GmbH, Germany) and following the set-up illustrated in figure 3. To reduce the number of time-consuming experiments done in a water tank, the relative water-equivalent path length of each material was derived using solid water WT1, in which a relative WT1-equivalent path length was obtained for each slab of thermoplastic. First, a percentage depth dose (PDD) curve was acquired in WT1 solid water material following a source-to-surface distance (SSD) approach, with an SSD of 100 cm and a field size of  $5 \times 5 \text{ cm}^2$  (100 MUs were delivered). Under the same SSD approach and keeping a constant 5 cm depth above the detector, the 3D-printed slabs were stacked together with WT1 solid water for point dose readings (figure 3). A bolus material was placed around the slabs to account for phantom scattering.



**Figure 2.** CT-scan set-up (images (a) and (b), coronal and axial planes, respectively) for the acquisition of average HU for each thermoplastic material (greyscale representing HU). For each material, the 1 cm and 2 cm slabs were stacked together and surrounded by solid water slabs and a bolus material (6 cm top, 6 cm bottom and sides) to account for phantom and backscatter. Images (c) and (d) show the ROI (red box, dimensions  $9.6 \times 9.6 \times 0.8 \text{ cm}^3$ ) defined in the axial and coronal planes, respectively, for a 1 cm thickness slab. For the slabs with 2 cm thickness, the ROI had a defined fixed thickness of 1.8 cm. Images (e) and (f) show, respectively, the HU distribution within the volume of a slab and HU profiles over the middle lines at the three axes (colour coded as per image (c) and (d)).





From the PDD curve obtained in WT1, relative WT1-equivalent path length values were extracted for each slab of thermoplastic. Then, the relative water-equivalent path length values for each sample were simply derived by multiplying the relative WT1-equivalent path length of the thermoplastic with the relative water-equivalent path length of WT1, which was measured, previously to this work, as 1.0068.

All proton beam irradiations were performed on the Varian ProBeam (Varian Medical Systems, CA, USA) installed at University College London Hospitals NHS Foundation Trust. The relative water-equivalent path length measurements of each 3D-printed slab was measured using the Giraffe detector (Ion Beam Applications SA, Belgium), which has a spatial geometric resolution of approximately 2 mm and a 0.5 mm uncertainty in the proton range determination. The Giraffe was placed on the treatment couch with the entrance window aligned with the isocentre, facing the nozzle. The samples were placed in front of the Giraffe with their centre aligned with the lasers. In

each irradiation, a single-spot pencil beam was delivered with fully retracted snout, following the set-up illustrated in figure 4. The Giraffe detector is calibrated to provide range information in water, and the water-equivalent path length corresponds to the shift in water between the Bragg peak curves measured with and without the sample in the beam path.

### 2.3. Comparison between CT predicted RED and RSP and measured values

To evaluate the CT characterisation errors in the treatment chain for each of the six thermoplastics, the calibration curves of each of the two independent CT scanners were used to predict average values for  $\rho$ , RED and RSP from the HU. The differences between predicted and measured values were reported, allowing us to determine if the thermoplastics are suitable to be used in end-to-end QA devices without requiring overrides in the TPS. Materials with differences below 5% were considered adequate for this application, in

agreement with other authors (Grant *et al* 2014, Lewis *et al* 2018, Tino *et al* 2022).

## 2.4. Comparison against theoretical properties of the 3D-printed thermoplastics

Theoretical prediction of the mass density and radiological properties of materials allows for rapid prototyping, identification, and selection of new tissue-equivalent materials before experimental characterisation. Theoretical values of  $\rho$ , RSP and RED for each of the six thermoplastic materials were estimated and compared against experimental values, to determine if one could use theoretical modelling to identify existing and/or develop new thermoplastics as tissue-substitute materials.

Both the density provided by the vendor and the extrusion multiplier were considered when estimating the theoretical  $\rho$  of the 3D-printed materials. The extrusion multiplier, also known as flow rate, is one of the 3D-printing parameters that strongly impacts the density of 3D-printed samples, as it defines the rate at which filament is extruded from the printer's nozzle (Ozsoykal and Yurt 2024). For each material, the extrusion multiplier should be optimised to avoid under- or over-extrusion of the printed layers. The theoretical mass density was obtained by multiplying the density of the filament as provided by the vendor with the extrusion multiplier  $(f_{EM})$ . Predicted values were generated using the optimised empirical value for the extrusion multiplier (table 1). We also provide a range of predicted  $\rho$  for the range of extrusion multipliers values used in this study (i.e.,  $f_{EM} = [0.85-1.0]$ ), since the optimal factor is unknown prior to experiments and can vary depending on the system used. A value of  $f_{EM} = 1$  was used when the empirical value was larger than 1 as the samples produced cannot be denser than the raw filament. The full range of theoretical  $\rho$  was used to obtain theoretical calculations of REDs and RSPs.

The theoretical RED and RSP values were calculated using a previously published mathematical model (Cook *et al* 2023) based on the elemental composition of the thermoplastics (table 1).

The RED of each material  $(RED_m)$  was calculated as the ratio between the electron density of the material  $(\rho_{e,m})$  and the electron density of water  $(\rho_{e,w})$ ,

$$RED_m = \rho_{e,m}/\rho_{e,w} \tag{1}$$

The electron density of the material was calculated as,

$$\rho_{e,m} = \rho_m N_A \left(\frac{Z}{A}\right)_{...} \tag{2}$$

where  $\rho_m$  is the mass density of the material (as provided by the vendor and adjusted with the extrusion multiplier) and  $N_A$  is the Avogadro number. The term  $\left(\frac{Z}{A}\right)_m$  is defined from the elemental composition of the material as  $\sum_i \left(\frac{\omega_i Z_i}{A_i}\right)$ , where  $Z_i$ ,  $A_i$  and  $\omega_i$  are

the atomic number, the atomic mass and the mass

fractional weight, respectively, of the component i of the composite material m. The element data ( $Z_i$  and  $A_i$ ) was taken from the ICRU report 37 (International Commission on Radiation Units and Measurements 1984).

The RSP of each material  $(RSP_m)$  was calculated as the ratio between the stopping power of the material  $(S_{col,m})$  and the stopping power of water  $(S_{col,w})$ ,

$$RSP_m = S_{col,m}/S_{col,w} (3)$$

The Bethe formula for heavy charged particles was used to derive the theoretical stopping powers,

$$S_{col,m} = \rho_m \frac{4\pi r_e^2 mc^2}{u} \frac{z^2}{\beta^2} \left(\frac{Z}{A}\right)_m$$

$$\times \left[ \ln \left(\frac{2mc^2\beta^2}{(1-\beta^2)I_m}\right) - \beta^2 \right]$$
(4)

where  $r_e$  is the classical electron radius,  $mc^2$  is the electron rest energy, u is the atomic mass unit,  $\beta$  is the velocity of the incident particle divided by the velocity of light, and z the charge of proton. The fundamental physical constant values from Cohen and Taylor (1987) were used in the calculations.  $I_m$  is the mean excitation energy of composite material m, and it was calculated using Bragg's additivity rule,  $\ln I_m = \left(\sum_i \frac{\omega_i Z_i}{A_i} \ln I_i\right) \left(\sum_i \frac{\omega_i Z_i}{A_i}\right)^{-1}$ , where  $I_i$  is the excitation energy of the component i of the composite material m, also taken from the ICRU report 37 (International Commission on Radiation Units and Measurements 1984). The proton RSP values were calculated for the experimental beam energy of 210 MeV.

# 2.5. Comparison against theoretical properties of biological tissues

The mass density and radiological properties of a variety of biological tissues were compared against the obtained experimental values for the thermoplastic materials, to determine the tissue-equivalence of each thermoplastic at diagnostic photon and therapeutic photon and proton energies.

The biological tissues considered were adipose, heart, grey matter (brain), lung (inflated), skeletal muscle and cortical bone of adults and, when possible, of children. Theoretical RED and RSP values were calculated using the mathematical model described in section 2.4 and the elemental compositions provided by White *et al* (1991). Theoretical values for  $\rho$  and HU were taken from White *et al* (1991) and McGarry *et al* (2020), respectively.

### 3. Results

# 3.1. Experimental values for mass density, RED and RSP and comparison against theoretical values

The measured data for  $\rho$ , RED and RSP of the six 3D-printable thermoplastic materials can be found in table 2, as well as comparisons against the theoretical values estimated mathematically. The measured  $\rho$ ,

Table 2. Measured and theoretical values for mass density, relative electron density and relative stopping power for each thermoplastic. Percentage differences were calculated between measured and theoretical values.

	Mass density $( ho)$			Relative electron density (RED)			Re	Relative stopping power (RSP)		
	Measured $[g/cm^3]$	Theoretical <sup>a [<math>g/cm^3</math>]</sup>	Diff[%]	Measured	Theoretical <sup>a</sup>	Diff[%]	Measured	Theoretical <sup>a</sup>	Diff[%]	
PLA	$1.116 \pm 0.008$	1.0800 [1.0200-1.2000]	3.23	$1.016 \pm 0.012$	1.029 [0.972–1.143]	1.28	$1.064 \pm 0.005$	1.025 [0.968–1.139]	3.67	
ABS	$0.954 \pm 0.003$	0.9360 [0.8840-1.0400]	1.89	$0.938 \pm 0.019$	0.913 [0.862-1.014]	2.67	$0.959 \pm 0.002$	0.928 [0.876-1.031]	3.23	
PETG	$1.038 \pm 0.007$	1.0795 [1.0795-1.2700]	4.00	$0.975 \pm 0.013$	1.029 [1.029-1.210]	5.54	$1.019 \pm 0.006$	1.030 [1.030-1.212]	1.08	
PMMA	$1.099 \pm 0.003$	1.0830 [0.9690-1.1400]	1.46	$1.011 \pm 0.022$	1.056 [0.944-1.111]	4.45	$1.083 \pm 0.004$	1.063 [0.951-1.119]	1.85	
HIPS	$0.912 \pm 0.005$	0.9975 [0.8925-1.0500]	9.38	$0.922 \pm 0.015$	0.981 [0.878-1.033]	6.40	$0.914 \pm 0.007$	1.000 [0.895-1.053]	9.41	
StoneFil	$1.562 \pm 0.003$	1.7000 [1.4450–1.7000]	8.83	$1.284 \pm 0.007$	1.567 [1.332–1.567]	22.04	$\boldsymbol{1.407 \pm 0.003}$	1.498 [1.273–1.498]	6.47	

<sup>&</sup>lt;sup>a</sup> theoretical mass density values reported for the extrusion multiplier ( $\mathbf{f}_{EM}$ ) used experimentally and for a typical range of values ( $\mathbf{f}_{EM} = [0.85-1.0]$ ). Abbreviations: PLA—Polylactic Acid; ABS—Acrylonitrile Butadiene Styrene; PETG—Polyethylene Terephthalate Glycol; PMMA—Polymethyl Methacrylate; HIPS—High Impact Polystyrene.

**Table 3.** Experimental Hounsfield Units (average  $\pm$  standard deviation) for each thermoplastic material derived using two independent CT scanners.

CT scanner	Hounsfield Units (HU)							
G1 scanner	PLA	ABS	PETG	PMMA	HIPS	StoneFil		
AnyScan TRIO® Philips Spectral 7500	$58 \pm 17$ $48 \pm 14$	$-90 \pm 12$ $-107 \pm 10$	$-34 \pm 19$ $-58 \pm 23$	$56 \pm 18$ $33 \pm 22$	$-134 \pm 16$ $-157 \pm 14$	$735 \pm 28$ $836 \pm 28$		

Abbreviations: PLA—Polylactic Acid; ABS—Acrylonitrile Butadiene Styrene; PETG—Polyethylene Terephthalate Glycol; PMMA—Polymethyl Methacrylate; HIPS—High Impact Polystyrene.

RED and RSP values, considering all materials, varied between [0.912-1.562] g cm<sup>-3</sup>, [0.922-1.284] and [0.914-1.407], respectively. The range of percentage differences calculated between measured and theoretical values were [1.46-9.38] %, [1.28-22.04] % and [1.08–9.41] % for  $\rho$ , RED and RSP respectively. Generally, the assumption of weighting the mass density by the extrusion multiplier was adequate for PLA, ABS, PETG and PMMA, with percentage differences between theoretical and measured values below 5%. For HIPS and Stonefil higher discrepancies were found, with the prediction over-estimating the density of the printed samples. When considering the data provided for RED and RSP, percentage differences below 5%, or just above, was found for all materials except HIPS and Stonefil, for which higher differences were found, with StoneFil reaching a difference of 22.04% for photon irradiation. In general, the theoretical calculations for RSP were closer to the experimental values than for RED.

### 3.2. Experimental Hounsfield Units

The HU values obtained for each thermoplastic with the two independent CT scanners are presented in table 3. Similar standard deviations were found for all materials and these fall under the order of magnitude of the variations intrinsic to CT systems, related to the selection of CT parameters and reconstruction algorithms (Davis *et al* 2018, Sorooshfard *et al* 2023). Stonefil was the material showing the highest standard deviations for both CT scanners.

# 3.3. Comparison between CT predicted RED and RSP and measured values

Figure 5 shows the HU to  $\rho$ , RSP and RED calibration curves for the AnyScan TRIO® and Philips Spectral 7500 CT scanners, together with the experimental measurements taken on these properties for each thermoplastic. For the AnyScan TRIO® scanner, the range of percentage differences calculated between the measured and CT predicted values, considering all materials, was [0.38–6.07] %, [0.10–15.34] % and [0.75–2.31] % for  $\rho$ , RED and RSP respectively. The range of percentage differences found for the Philips scanner was [0.22–3.78] %, [1.64–9.42] % and [0.11–5.36] % for  $\rho$ , RED and RSP respectively. In

general, a good agreement was found between CT predicted and measured mass densities and RSPs in both CT scanners for most materials—only the predicted RSP for PMMA and the predicted  $\rho$  for PETG showed percentage differences slightly above 5% (5.36% and 6.07%, respectively) and only for one of the two scanners. The CT calibration curves also predicted well the RED, with percentage differences below 5% for all materials except Stonefil, associated with the highest differences for both scanners (9.42% and 15.34%) and HIPS with a 6.94% difference for the Philips 7500 scanner. Full data can be found in Supplementary Material table S1.

### 3.4. Comparison against biological tissues

Figure 6 shows the  $\rho$ , RED, RSP and HU values for a variety of biological tissues (theoretical values) and the six thermoplastics (experimental values) analysed in this study. Full data for the biological tissues can be found in Supplementary Material table S2. Stonefil showed properties closer to the ones of cortical bone, especially for a 5-year-old child, with differences of 10.74%, 21.80% and 10.72% for  $\rho$ , RED and RSP, respectively, and HU within the theoretical range. The properties of PLA, ABS, PETG, PMMA and HIPS were closer to soft tissues. ABS closely matched adipose tissue, showing differences of 0.42%, 1.68% and 1.24% for  $\rho$ , RED, and RSP, respectively, compared to adult adipose tissue and differences of 0.93%, 2.90% and 1.94% for  $\rho$ , RED and RSP, respectively, compared to child adipose tissue. The average HU value found for ABS was also close to the lower limit (-85 HU) of the range reported for adipose tissue, with 5.88% difference. The properties obtained for PLA, PETG and PMMA had also good proximity with the ones of skeletal muscle, and brain, for both adult and paediatric tissues (percentage differences below 8.35%, 6.70% and 5.25% for  $\rho$ , RED, RSP, respectively). No thermoplastic had comparable properties to lung (inflated).

### 4. Discussion

In this work, we evaluated the potential of a variety of commercially available 3D-printable thermoplastics as tissue-equivalent materials for multimodality

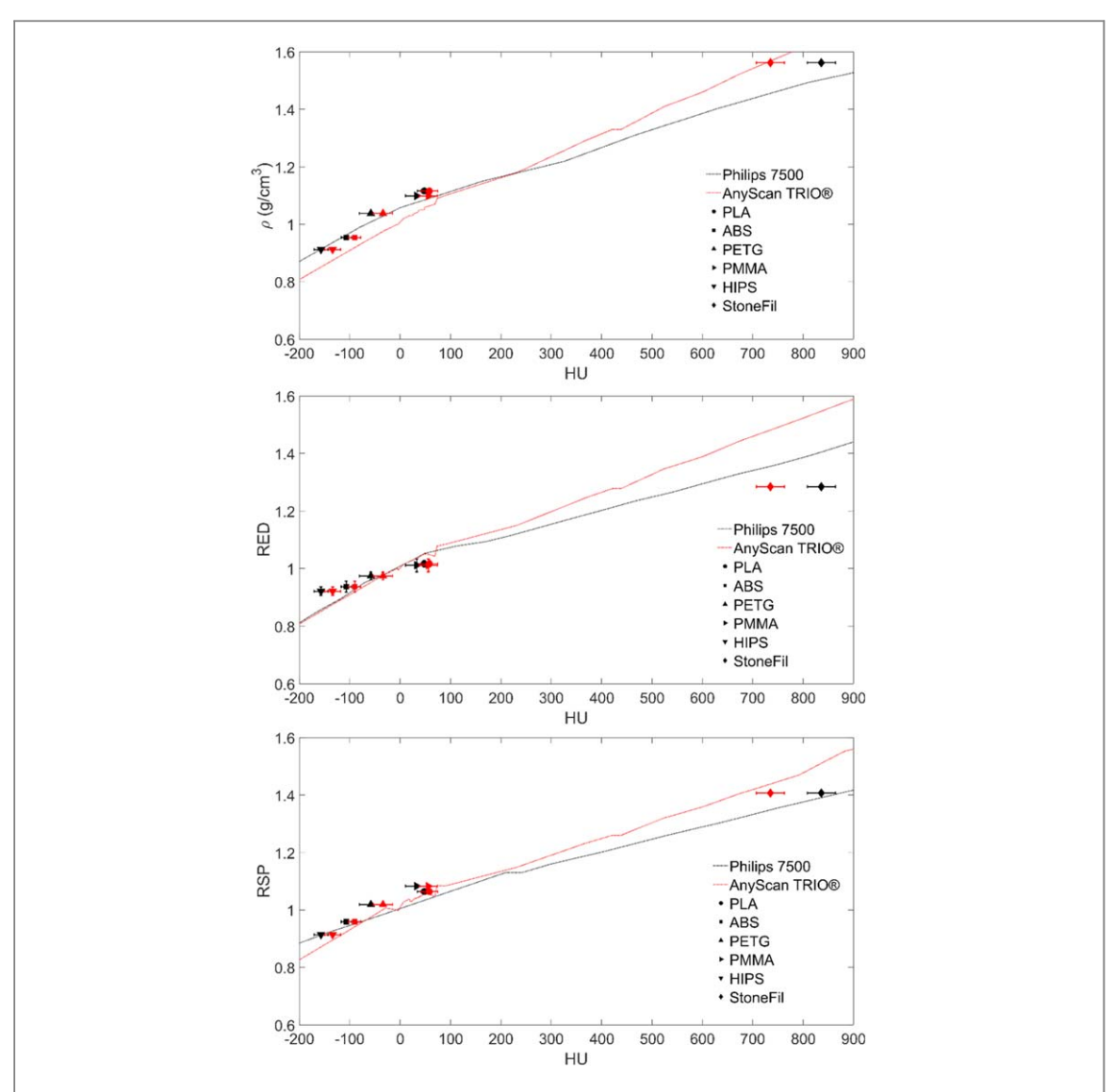


Figure 5. Hounsfield Units (HU) to mass density ( $\rho$ ), relative electron density (RED) and relative stopping power (RSP) calibration curves for the Philips 7500 and AnyScan TRIO\* scanners (black and red lines, respectively). The data points correspond to the experimental measurements for each thermoplastic. Abbreviations: PLA—Polylactic Acid; ABS—Acrylonitrile Butadiene Styrene; PETG—Polyethylene Terephthalate Glycol; PMMA—Polymethyl Methacrylate; HIPS—High Impact Polystyrene.

end-to-end radiotherapy QA purposes. We found errors between CT predicted and measured values below 5% for several thermoplastic materials as well as similarity with a variety of biological tissues in terms of mass density, relative electron density and relative stopping power. Furthermore, theoretical predictions of these properties were shown to be useful to identify similarities between materials and target biological tissues before experiments are performed. To the best of our knowledge, this is the first time that a variety of 3D-printable thermoplastics were comprehensively evaluated for the whole radiotherapy treatment chain, while considering both photon and proton beam modalities.

The  $\rho$ , RED and RSP values were predicted for a variety of commercially available 3D-printable thermoplastics using the calibration curves of two independently commissioned CT scanners and compared against experimental measurements. For the  $\rho$  and

RSP values percentage differences were below or slightly above 5% for the investigated thermoplastics. The six thermoplastic materials evaluated in this work are therefore suitable candidates for end-to-end QA in proton beam therapy, with no overrides required during the dose calculation step by the TPS to achieve an accuracy within  $\pm 5\%$ . As for photon beam therapy, PLA, ABS, PETG and PMMA were also promising. A difference of 6.94% was found for HIPS predicted RED, but again only for one of the two scanners. However, the use of different CT scan calibration curves can result in differences up to around 2% between calculated and measured absolute dose values (Hasani et al 2019). Therefore, HIPS should not be completely discarded as tissue-equivalent material for end-to-end QA phantoms in photon beam therapy. Stonefil showed significant differences between the CT predicted and measured RED values for both scanners (9.42% and 15.34%), likely due to the presence of high

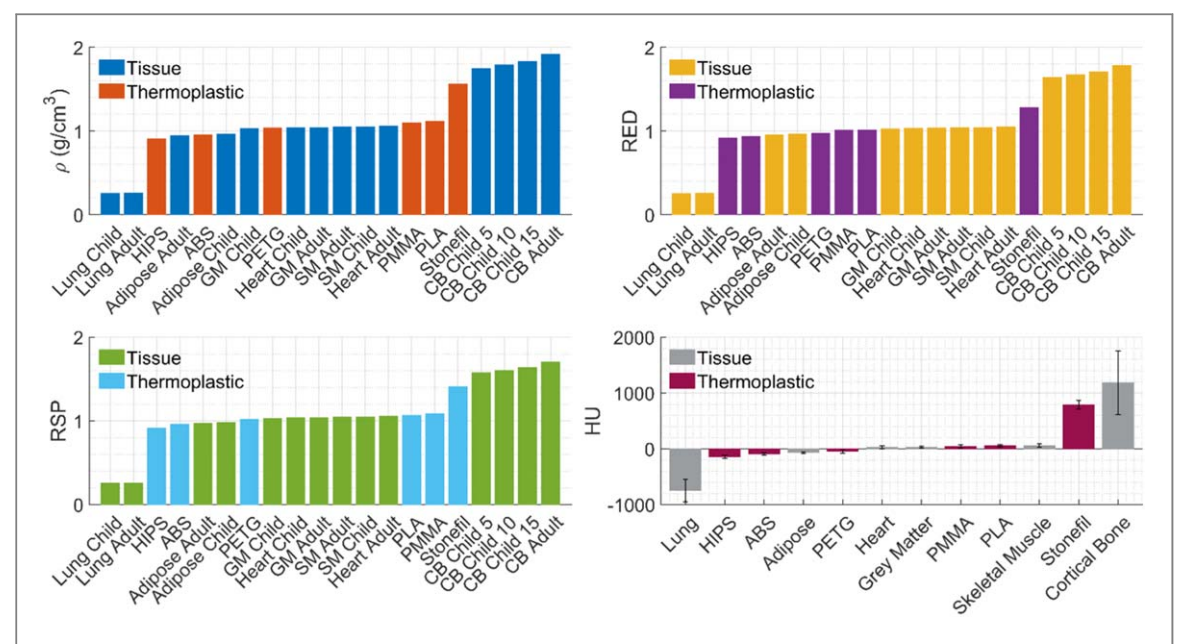


Figure 6. Waterfall plots of experimental (thermoplastics) and theoretical (biological tissues) values for mass density, relative electron density, relative stopping power and Hounsfield Units. Abbreviations: PLA—Polylactic Acid; ABS—Acrylonitrile Butadiene Styrene; PETG—Polyethylene Terephthalate Glycol; PMMA—Polymethyl Methacrylate; HIPS—High Impact Polystyrene; GM—Grey Matter; SM—Skeletal Muscle; CB—Cortical Bone.

Z elements in its composition. The presence of high Z elements can result in a higher number of photoelectric interactions at diagnostic energies, with increased photon attenuation and consequent higher prediction of the material's RED. For proton irradiation, the interaction of particles with a medium is most influenced by its density. Therefore, HU to RSP calibration curves can do well, even if HU to RED predictions are poor, highlighting how tissue-equivalent materials tailored for end-to-end QA in photon therapy might not be suitable for application in proton beam therapy, and vice-versa.

The materials considered in this study have good potential to act as substitutes for a variety of biological tissues. StoneFil was the best candidate for a bone equivalent material due its higher density value, being the closest match to paediatric bone tissues. However, its properties were at least 10% lower than all bone materials investigated, indicating the need for the development of denser bone equivalent thermoplastic materials. The production of bone materials is still a challenging process that requires optimisation, as these are the tissue-equivalent materials with the most significant uncertainties in dose measurements (Lewis et al 2018, Cook et al 2023). ABS was found to be a good substitute for adipose tissue, with percentage differences below 3% for all properties. PLA, PETG and PMMA were good candidates to substitute skeletal muscle and brain tissues. In general, PLA performed better for photon therapy whilst PETG had better equivalency for proton therapy (RED and RSP percentage differences below 3% and 2.5%, respectively, for the two tissue types). For the lung tissue (inflated) specifically, no thermoplastic had

comparable properties due to the presence of air in the lungs. With 3D-printing it is possible to decrease the density of the models by tweaking the 3D-printing parameters and choosing lower percentages for infill patterns. Kairn et al (2015) have demonstrated in their work that ABS 3D-printed at an infill percentage in the range of 30% to 50% create enough air volume in the core of the phantom to closely mimic lung under photon irradiation. However, there are additional challenges associated with increasing volume of air gaps in a patterned infill, especially for proton particles. Botnariuc et al (2022) have highlighted, using Monte Carlo simulations, that for lower infill percentages, the direction of the printing pattern relative to the proton beam (parallel versus perpendicular) impact the range of proton particles and consequently the final dose distributions.

Small HU standard deviations were found for all materials and these are under the order of magnitude of the variations intrinsic to CT systems, related to the selection of CT parameters and reconstruction algorithms (Davis et al 2018, Sorooshfard et al 2023). This finding indicated good reproducibility in the manufacturing of the 3D-printing slabs as well as the ability of achieving a uniform density distribution within the volume of each individual slab. Reproducibility and uniformity are important aspects in the development of dosimetry physical phantoms to guarantee reproducibility in the measurements. To achieve dense, homogeneous samples we opted to use 'Solid Layers' as infill type in the production of our 3D-printed samples, together with the correct tuning of the extrusion multiplier. Madamesila et al (2016) investigated various infill patterns using CT imaging, and large HU

variations were found except for when the 'Lines' pattern was used. While it is unclear how similar their 100% filled 'Lines' pattern and our 'Solid Layers' are, as different splicing software were used, our findings together indicate that more densely filled patterns are more suitable for the 3D-printing of phantoms for dosimetry purposes in radiotherapy. Stonefil was the material showing the biggest variations in HU, in agreement with studies by Davis et al (2018) and Sorooshfard et al (2023) where larger variations were also reported for bone-like materials. The HU obtained for PLA and ABS in the present work are comparable with values obtained in other studies. Dancewicz et al (2017) reported HU of 8  $\pm$  4 and  $-113 \pm 3$  for 3D-printed samples made of PLA and ABS, respectively, with 90% infill. These values are slightly below the ones found in the present work for the same materials, which agrees with the lower infill percentage used of 90% compared to our Solid Layers infill type. Van der Walt et al (2019) have also provided HU of 138  $\pm$  12 for PLA samples printed with a rectilinear pattern and 100% infill.

3D-printing has great potential to disrupt how phantoms are manufactured for end-to-end quality assurance of diagnostic and therapeutic radiation modalities. The accuracy at which phantoms mimic the human body depends on how realistic they are in terms of composition and anatomical shape. With recent advances in 3D-printing (e.g., multi-filament printing and material doping) it is becoming possible for clinics to create in-house increasingly complex and realistic phantoms at reduced costs (Han and Lee 2020, Price et al 2020, Hasanov et al 2022, Fonseca et al 2023). There is a particular need for the development of novel lung and bone tissue-equivalent materials, as well as materials that are suitable for different radiation applications (e.g., diagnostic and therapeutic modalities).

A mathematical model, developed to calculate theoretical values of radiological properties, was also evaluated for the selection of potential future tissueequivalent materials in therapeutic photon and proton beams. Being able to accurately estimate mass density and radiological properties from tabulated data would be very useful to guide researchers in the design/prototyping of novel tissue-equivalent materials through filament doping (Price et al 2020), and for clinics to evaluate the potential of existing and upcoming commercially available materials, reducing the time spent on iterative trial-and-error and experiments. The mathematical model showed promise in the calculation of radiological properties for most of the 3Dprinting materials and may be a useful tool to support the selection of other materials as tissue-equivalent materials. However, the model's performance is highly dependent on accuracy of the elemental composition and densities used for the calculations. Commercially available filaments are likely to contain impurities and manufacturers typically do not provide information

regarding the exact elemental compositions of their filaments. HIPS and Stonefil had the highest mismatch between the measured and predicted mass densities (even after weighting by the extrusion multiplier), which reflected on the highest mismatch between the theoretical and measured radiological properties. Furthermore, when considering a new thermoplastic as a potential tissue substitute, it is important to take into consideration a range of predicted mass density values for a better insight on the post-printing properties of the models. Van der Walt et al (2019) have measured a post-printing mass density of 1.173 g cm<sup>-3</sup> for PLA samples, printed with an extrusion multiplier of 1, a rectilinear pattern and a filament's density of 1.27 g cm<sup>-3</sup>. Even though a higher extrusion rate was selected, a similar reduction in density was found in comparison to the present work (7.64% versus 7% PLA density reduction post-printing). Further tests should therefore be performed to better understand the correlation between printing parameters, like the extrusion multiplier and infill patterns, and the post-printing density for different thermoplastics. Additionally, some materials might behave differently when extruded—StoneFil showed the highest mismatch between densities despite an extrusion multiplier larger than one being used. This might suggest a limitation of the 3D printer to perform at an extrusion flow rate beyond a maximum threshold.

Our study has certain limitations. Only six thermoplastic materials were analysed but a large variety of filaments is commercially available nowadays, as well as doped and personalised 3D-printable materials. Dancewicz et al (2017) analysed PLA doped with bronze, copper and wood fibres and these materials presented very distinct mass densities and HU from the ones obtained for the six materials analysed in this study. We have only evaluated the thermoplastic materials in one colour; however, vendors produce filaments typically in a variety of colours and other studies have shown that radiological properties can vary due to the pigments and other additives used (Fonseca et al 2023). Therefore, caution must be taken when generalising our findings to other thermoplastics. Another limitation includes the fact that only two CT scanners were used in the evaluation of how well calibration curves predict properties for thermoplastic materials. Testing our samples in a larger variety of number of scanners would provide greater confidence on the biological equivalence of the materials at diagnostic energy levels, namely those with percentage differences close to 5%. Finally, we only considered the impact of the extrusion multiplier in the mass density, but other printing parameters are likely to affect the density achieved. In addition to the impact of choice of extrusion multiplier (Ozsoykal and Yurt 2024), printing speed and nozzle diameter have been discussed by Marshall et al (2023) as additional parameters with great impact on the final post-printing density of models. Slower printing speed might increase the final

mass density of the samples, by allowing for more extrusion per time, but it compromises on longer printing times that might not be acceptable in clinical settings. In the present study, we adjusted the varied printing parameters to values that would allow the best printing quality. The extrusion multiplier was selected in last and optimised to avoid under- and over-extrusion under the set of values already defined for the remaining parameters. Nevertheless, our approach to calculate theoretical mass densities may be too simplified and only applicable to our 3D printer settings; additional printing factors should be explored for these theoretical calculations.

Even though 3D-printing technology has great potential for the manufacturing of high-quality physical phantoms for end-to-end QA in radiotherapy, bringing flexibility and customisation at reduced costs, further work is required to fully characterise and understand this technology for the application before it can replace traditional manufacturing techniques. The presence of air gaps in the models' filling, imperfect infill density uniformity, small building volumes, poorer surface finishing and limited range number of commercially available filaments are some of the disadvantages associated with 3D-printing. Moreover, considerations regarding plastic waste need to be accounted for. A printing plan should be developed to prevent failed prints and more research is required to understand the long-term viability of 3D-printing phantoms and how the thermoplastic properties are likely to change over years of continuous radiation exposure. Van der Walt et al (2019) have reported no alterations on the geometric dimensions of 3D-printed samples with PLA, after one month of exposure to doses extensively higher than the ones delivered during treatments. However, no investigation was done on changes to their radiological properties. Additional work is also required on the development of guidelines for the 3D-printing of good quality phantoms. In a recent study by Marshall et al (2023), a 3D-printed phantom designed for the QA of a six degrees-of-freedom treatment couch was 3D-printed in five different centres using PLA. Even though instructions were provided regarding infill patterns and percentages, the selection of the remaining 3D-printing parameters were defined individually by each institution. Different PLA HU were found for the phantoms developed in the different centres (range: 150-200, approximately), demonstrating that models produced with the same infill choices (e.g., pattern and infill percentage), but using different printers and parameters, will produce phantoms with distinct final post-printing density and radiological properties at imaging energy levels. Moreover, one should consider that different printers, working with the same parameters, are likely to perform differently and print samples with different properties. A set of parameters will not be optimal for all 3D-printers and the implementation of a workflow to guide on the tuning of parameters on each 3D-

printer individually should be developed locally to minimise some of the limitations associated with 3Dprinting for the development of good quality phantoms for radiotherapy.

### 5. Conclusions

This work demonstrated the potential of using 3Dprinted thermoplastics in the development of physical phantoms for photon and proton beam therapy. The samples production was reproducible and presented uniform mass density distribution. Several 3D-printed thermoplastics were found to be promising tissueequivalent materials for multimodal end-to-end radiotherapy QA phantoms and will not require corrections in treatment planning systems for dose calculations. Stonefil was the best bone equivalent candidate for proton irradiation (in particular for paediatric patients) but differences were larger than 5%. ABS may be used as a substitute for adipose tissue for both modalities. PETG and PLA were good candidates to be skeletal muscle, brain and lung tissueequivalent materials for both modalities. The mathematical model was a useful tool to investigate potential materials to be used as tissue equivalents, as long as correct information on the post-printing density and elemental composition on the materials is provided.

### Acknowledgments

This work was supported by The Royal Society Research Grants (RGS/R2/202025). CV was supported by the Royal Academy of Engineering under the Research Fellowship scheme (RF\201718\17140). The work performed at NPL was supported by the National Measurements System Programmes Unit of the UK's Department for Science, Innovation and Technology. The authors would like to acknowledge Alex Douralis for helping with the measurements in photon therapeutic energies and Kelley Ferreira for helping with the CT scan acquisitions.

### Data availability statement

The data cannot be made publicly available upon publication because the cost of preparing, depositing and hosting the data would be prohibitive within the terms of this research project. The data that support the findings of this study are available upon reasonable request from the authors.

### **ORCID** iDs

Mariana Bento https://orcid.org/0000-0003-3345-8985
Hannah Cook https://orcid.org/0000-0002-3306-9704

- Virginia Marin Anaya https://orcid.org/0000-0001-7844-7759
- Ana Lourenço https://orcid.org/0000-0001-6829-3338
- Mohammad Hussein https://orcid.org/0000-0002-1597-740X
- Catarina Veiga https://orcid.org/0000-0002-4132-2554

### References

- Alexander K M, Dekker K H, Olding T and Schreiner L J 2022 Endto-end quality assurance of stereotactic radiation therapy using an anthropomorphic head phantom *J. Phys. Conf. Ser.* 2167 012022
- Allahverdi M, Nisbet a and Thwaites D I 1999 An evaluation of epoxy resin phantom materials for megavoltage photon dosimetry *Phys. Med. Biol.* **44** 1125
- Arjomandy B, Sahoo N, Zhu X R, Zullo J R, Wu R Y, Zhu M, Ding X, Martin C, Ciangaru G and Gillin M T 2009 An overview of the comprehensive proton therapy machine quality assurance procedures implemented at The University of Texas M D Anderson Cancer Center Proton Therapy Center–Houston Med. Phys. 36 2269–82
- Arjomandy B et al 2019 AAPM task group 224: comprehensive proton therapy machine quality assurance Med. Phys. 46 e678–705
- Baskar R, Lee K A, Yeo R and Yeoh K-W 2012 Cancer and radiation therapy: current advances and future directions *Int. J. Med. Sci.* 9 193–9
- Botnariuc D, Ghica C, Cook H, Bento M, Nisbet a, Royle G, Hussein M and Lourenço A 2022 A Monte Carlo framework to evaluate the radiological properties of 3D- printable materials for proton therapy phantom development International Conference on Monte Carlo Techniques for Medical Applications (MCMA)
- Brunner J, Langgartner L, Danhel H, Birkfellner W, Richter C, Wagenaar D, Stock M, Georg D and Knäusl B 2024
  Dosimetric characteristics of 3D-printed and epoxy-based materials for particle therapy phantoms *Front. Phys.* 12
  1323788
- Burleson S, Baker J, Hsia A T and Xu Z 2015 Use of 3D printers to create a patient-specific 3D bolus for external beam therapy *J. Appl. Clin. Med. Phys.* 16 5247
- Cheung K 2006 Intensity modulated radiotherapy: advantages, limitations and future developments *Biomed. Imaging Interv J.* 2 e19
- Chung J P, Seong Y M, Kim T Y, Choi Y, Kim T H, Choi H J,
  Min C H, Benmakhlouf H, Chun K J and Chung H-T 2018
  Development of a PMMA phantom as a practical alternative
  for quality control of gamma knife® dosimetry *Radiation*Oncology 13 176
- Cohen E R and Taylor B N 1987 The 1986 adjustment of the fundamental physical constants *Rev. Mod. Phys.* **59** 1121–48
- Constantinou C, Attix F H and Paliwal B R 1982 A solid water phantom material for radiotherapy x-ray and  $\gamma$ -ray beam calibrations *Med. Phys.* 9 436–41
- Cook H, Lambert J, Thomas R, Palmans H, Hussein M, Clark C H, Royle G, Pettingell J and Lourenço A 2022 Development of a heterogeneous phantom to measure range in clinical proton therapy beams *Physica Med.* 93 59–68
- Cook H et al 2023 Development of optimised tissue-equivalent materials for proton therapy Phys. Med. Biol. 68 075009
- Craft D F and Howell R M 2017 Preparation and fabrication of a full-scale, sagittal-sliced, 3D-printed, patient-specific radiotherapy phantom J. Appl. Clin. Med. Phys. 18 285–92

- Dancewicz O L, Sylvander S R, Markwell T S, Crowe S B and Trapp J V 2017 Radiological properties of 3D printed materials in kilovoltage and megavoltage photon beams *Physica Med.* 38 111–8
- Davis A T, Palmer A L, Pani S and Nisbet a 2018 Assessment of the variation in CT scanner performance (image quality and Hounsfield units) with scan parameters, for image optimisation in radiotherapy treatment planning *Physica Med.* 45 59–64
- Delombaerde L, Petillion S, Weltens C, De Roover R, Reynders T and Depuydt T 2020 Technical note: development of 3D-printed breast phantoms for end-to-end testing of whole breast volumetric arc radiotherapy *J. Appl. Clin. Med. Phys.* 21 315–20
- Ehler E D, Barney B M, Higgins P D and Dusenbery K E 2014 Patient specific 3D printed phantom for IMRT quality assurance *Phys. Med. Biol.* **59** 5763
- Fonseca G P, Rezaeifar B, Lackner N, Haanen B, Reniers B and Verhaegen F 2023 Dual-energy CT evaluation of 3D printed materials for radiotherapy applications *Phys. Med. Biol.* **68** 035005
- Fraass B, Doppke K, Hunt M, Kutcher G, Starkschall G, Stern R and Van Dyke J 1998 American association of physicists in medicine radiation therapy committee task group 53: quality assurance for clinical radiotherapy treatment planning *Med. Phys.* 25 1773–829
- Gargett M A, Briggs A R and Booth J T 2020 Water equivalence of a solid phantom material for radiation dosimetry applications Physics and Imaging in Radiation Oncology 14 43–7
- Grant R L, Summers P A, Neihart J L, Blatnica A P, Sahoo N, Gillin M T, Followill D S and Ibbott G S 2014 Relative stopping power measurements to aid in the design of anthropomorphic phantoms for proton radiotherapy *J. Appl. Clin. Med. Phys.* **15** 4523
- Han D and Lee H 2020 Recent advances in multi-material additive manufacturing: methods and applications *Current Opinion in Chemical Engineering* 28 158–66
- Hasani M, Farhood B, Ghorbani M, Naderi H, Saadatmand S, Karimkhani Zandi S and Knaup C 2019 Effect of computed tomography number-relative electron density conversion curve on the calculation of radiotherapy dose and evaluation of Monaco radiotherapy treatment planning system *Australas. Phys. Eng. Sci. Med.* 42 489–502
- Hasanov S, Alkunte S, Rajeshirke M, Gupta A, Huseynov O, Fidan I, Alifui-Segbaya F and Rennie A 2022 Review on additive manufacturing of multi-material parts: progress and challenges *Journal of Manufacturing and Materials Processing* 64
- Hassan M H, Omar A M, Daskalakis E, Hou Y, Huang B, Strashnov I, Grieve B D and Bártolo P 2020 The potential of polyethylene terephthalate glycol as biomaterial for bone tissue engineering *Polymers (Basel)* 12 3045
- International Commission on Radiation Units and Measurements 1984 Stopping Powers for Electrons and Positrons (Internat. Comm. on Radiation Units and Measurements)
- Ju S G, Kim M K, Hong C-S, Kim J S, Han Y, Choi D H, Shin D and Lee S B 2014 New technique for developing a proton range compensator with use of a 3-dimensional printer *Int. J. Radiat. Oncol. Biol. Phys.* 88 453–8
- Kadoya N, Abe K, Nemoto H, Sato K, Ieko Y, Ito K, Dobashi S, Takeda K and Jingu K 2019 Evaluation of a 3D-printed heterogeneous anthropomorphic head and neck phantom for patient-specific quality assurance in intensity-modulated radiation therapy *Radiol. Phys. Technol.* 12 351–6
- Kairn T, Crowe S B and Markwell T 2015 Use of 3D printed materials as tissue-equivalent phantoms World Congress on Medical Physics and Biomedical Engineering IFMBE Proceedings 51 ed D A Jaffray (Springer International Publishing) 728–31
- Kutcher G J et al 1994 Comprehensive QA for radiation oncology: report of AAPM radiation therapy committee task group 40 Med. Phys. 21 581–618

- Leary M, Kron T, Keller C, Franich R, Lonski P, Subic A and Brandt M 2015 Additive manufacture of custom radiation dosimetry phantoms: an automated method compatible with commercial polymer 3D printers *Mater. Des.* **86** 487–99
- Lewis D J, Taylor P A, Followill D S, Sahoo N, Mahajan A, Stingo F C and Kry S F 2018 A new anthropomorphic pediatric spine phantom for proton therapy clinical trial credentialing *Int. J. Part Ther.* 4 20–7
- Liu H and Chang J Y 2011 Proton therapy in clinical practice Chin. J. Cancer 30 315–26
- Lomax A 1999 Intensity modulation methods for proton radiotherapy Phys. Med. Biol. 44 185
- Madamesila J, McGeachy P, Villarreal Barajas J E and Khan R 2016 Characterizing 3D printing in the fabrication of variable density phantoms for quality assurance of radiotherapy Physica. Med. 32 242–7
- Mármol I, Ballester P, Cerro S, Monrós G, Morales J and Sánchez L 2010 Use of granite sludge wastes for the production of coloured cement-based mortars *Cem. Concr. Compos.* **32** 617–22
- Marshall H, Selvan T, Ahmad R, Bento M, Veiga C, Sands G,
  Malone C, King R B, Clark C H and McGarry C K 2023
  Evaluation of a novel phantom for the quality assurance of a
  six-degree-of-freedom couch 3D-printed at multiple centres
  Physica. Med. 114 103136
- McGarry C K et al 2020 Tissue mimicking materials for imaging and therapy phantoms: a review Phys. Med. Biol. 65 23TR01
- Moutrie V, Kairn T, Rosenfeld A and Charles P H 2015 Use of a megavoltage electronic portal imaging device to identify prosthetic materials *Australas*. *Phys. Eng. Sci. Med.* 38 93–100
- Mutic S, Palta J R, Butker E K, Das I J, Huq M S, Loo L-N D, Salter B J, McCollough C H and Van Dyk J 2003 Quality assurance for computed-tomography simulators and the computed-tomography-simulation process: report of the AAPM radiation therapy committee task group No 66 Med. Phys. 30 2762–92
- Nakayenga J, Cikmit A A, Tsuchida T and Hata T 2021 Influence of stone powder content and particle size on the strength of cement-treated clay *Constr. Build. Mater.* 305 124710
- Oh D, Hong C-S, Ju S G, Kim M, Koo B Y, Choi S, Park H C, Choi D H and Pyo H 2017 Development of patient-specific phantoms for verification of stereotactic body radiation therapy planning in patients with metallic screw fixation *Sci. Rev.* 7 40922
- Ozsoykal I and Yurt A 2024 Introduction of a novel technique in density-adjusted 3D printing for the manufacture of softtissue-equivalent radiological phantoms *Applied Sciences* 14 509
- Paganetti H 2012 Range uncertainties in proton therapy and the role of Monte Carlo simulations *Phys. Med. Biol.* **57** R99–117
- Palma D, Vollans E, James K, Nakano S, Moiseenko V, Shaffer R, McKenzie M, Morris J and Otto K 2008 Volumetric modulated arc therapy for delivery of prostate radiotherapy: comparison with intensity-modulated radiotherapy and three-dimensional conformal radiotherapy *International Journal of Radiation Oncology\*Biology\*Physics* 72 996–1001
- Panneerselvam T, Raghuraman S and Vamsi Krishnan N 2021 Investigating mechanical properties of 3D-printed polyethylene terephthalate glycol material under fused deposition modeling *J. Inst. Eng. India Ser.* C 102 375–87
- Particle Therapy Co-Operative Group (PTCOG) 2024 Accessed Online https://ptcog.site/
- Price G et al 2020 An open source heterogeneous 3D printed mouse phantom utilising a novel bone representative thermoplastic Phys. Med. Biol. 65 10NT02
- Rana S, Bennouna J, Samuel E J J and Gutierrez A N 2019 Development and long-term stability of a comprehensive daily QA program for a modern pencil beam scanning (PBS)

- proton therapy delivery system *Journal of Applied Clinical Medical Physics* **20** 29–44
- Ranakoti L, Gangil B, Mishra S K, Singh T, Sharma S, Ilyas R A and El-Khatib S 2022 Critical review on polylactic acid: properties, structure, processing, biocomposites, and nanocomposites *Materials* 15 4312
- Rooney M K, Rosenberg D M, Braunstein S, Cunha A, Damato A L, Ehler E, Pawlicki T, Robar J, Tatebe K and Golden D W 2020 Three-dimensional printing in radiation oncology: A systematic review of the literature *J. Appl. Clin. Med. Phys.* 21
- Salimi M, Pirouzfar V and Kianfar E 2017 Enhanced gas transport properties in silica nanoparticle filler-polystyrene nanocomposite membranes Colloid Polym. Sci. 295 215–26
- Schneider U, Pedroni E and Lomax A 1996 The calibration of CT Hounsfield units for radiotherapy treatment planning *Phys. Med. Biol.* 41 111
- Schreiner L J 2019 End to end QA in image guided and adaptive radiation therapy *J. Phys. Conf. Ser.* **1305** 012062
- Sorooshfard E, Tahmasbi M, Chegeni N and Tahmasebi Birgani M J 2023 Evaluating the effects of variation in CT scanning parameters on the image quality and Hounsfield units for optimization of dose in radiotherapy treatment planning: A semi-anthropomorphic thorax phantom study *J. Cancer Res. Ther.* 19 426–34
- Stieler F, Wolff D, Schmid H, Welzel G, Wenz F and Lohr F 2011 A comparison of several modulated radiotherapy techniques for head and neck cancer and dosimetric validation of VMAT *Radiother. Oncol.* **101** 388–93
- Tillery H *et al* 2022 Personalized 3D-printed anthropomorphic whole-body phantom irradiated by protons, photons, and neutrons *Biomed. Phys. Eng. Express* 8 027004
- Tino R B, Yeo A U, Brandt M, Leary M and Kron T 2022 A customizable anthropomorphic phantom for dosimetric verification of 3D-printed lung, tissue, and bone density materials *Med. Phys.* 49 52–69
- Tino R, Yeo A, Leary M, Brandt M and Kron T 2019 A systematic review on 3D-printed imaging and dosimetry phantoms in radiation therapy *Technol. Cancer Res. Treat.* **18** 1533033819870208
- Van der Walt M, Crabtree T and Albantow C 2019 PLA as a suitable 3D printing thermoplastic for use in external beam radiotherapy *Australas*. *Phys. Eng. Sci. Med.* **42** 1165–76
- White D R, Widdowson E M, Woodard H Q and Dickerson J W 1991 The composition of body tissues (II). Fetus to young adult *Br. J. Radiol.* 64 149–59
- Yea J W, Park J W, Kim S K, Kim D Y, Kim J G, Seo C Y, Jeong W H, Jeong M Y and Oh S A 2017 Feasibility of a 3D-printed anthropomorphic patient-specific head phantom for patientspecific quality assurance of intensity-modulated radiotherapy *PLoS One* 12 e0181560
- Yushkevich P A, Piven J, Hazlett H C, Smith R G, Ho S, Gee J C and Gerig G 2006 User-guided 3D active contour segmentation of anatomical structures: significantly improved efficiency and reliability *Neuroimage* 31 1116–28
- Żenkiewicz M, Rytlewski P, Moraczewski K, Stepczyńska M, Karasiewicz T, Malinowski R and Ostrowicki W 2009 Some effects of multiple injection moulding on selected properties of ABS Journal of Achievements in Materials and Manufacturing Engineering 37 361–368
- Zhang R and Newhauser W D 2009 Calculation of water equivalent thickness of materials of arbitrary density, elemental composition and thickness in proton beam irradiation *Phys. Med. Biol.* **54** 1383–95
- Zou W *et al* 2015 Potential of 3D printing technologies for fabrication of electron bolus and proton compensators *J. Appl. Clin. Med. Phys.* 16 90–8